Journal of Volcanology and Geothermal Research 433 (2023) 107730

Contents lists available at ScienceDirect

Journal of Volcanology and Geothermal Research

journal homepage: www.journals.elsevier.com/journal-of-volcanology-and-geothermal-research

Temporal evolution of the Fogo Volcano magma storage system (Cape Verde Archipelago): a fluid inclusions perspective

Francesco Maria Lo Forte [a], Alessandro Aiuppa [a], Silvio G. Rotolo [a,b], Vittorio Zanon [c,*]

[a] Dipartimento di Scienze della Terra e del Mare, Università degli Studi di Palermo, 90123, Italy
[b] Istituto Nazionale di Geofisica e Vulcanologia, Sezione di Palermo, Via U. La Malfa 153, 90146 Palermo, Italy
[c] Instituto de Investigação em Vulcanologia e Avaliação de Riscos, Universidade dos Açores, Rua Mãe de Deus, 9500-321 Ponta Delgada, Portugal

ARTICLE INFO

Keywords:
Oceanic island volcanism
Magma ascent path
Basanites
Magmatic system

ABSTRACT

The architecture of the magma storage system underneath Fogo Volcano (Cape Verde Archipelago) is characterised using novel fluid inclusion results from fifteen basanites, spanning the last 120 thousand years of volcanic activity, and encompassing a major flank collapse event at ~73 ka. Fluid inclusions, hosted in olivine and clinopyroxene, are made of pure CO_2, and based on their textural characteristics, are distinguished in early (Type I) and late (Type II) stage. Inclusions homogenize to a liquid phase in the 2.8 to 30.8 °C temperature range. Densities values, recalculated assuming an original 10% H_2O content at the time of trapping, range from 543 to 952 kg·m^{-3}, and correspond to entrapment or re-equilibration pressure ranges of 500–595 MPa, 700–740 MPa, and 245–610 MPa respectively for pre-collapse, early post-collapse, and Holocene/historical eruptions. These entrapment pressures are interpreted as reflecting the existence of two main magma accumulation zones at ~25 km and ~ 13–21 km depth, and a zone of fluid inclusion re-equilibration at 9–12 km depth. There is evidence of a complex temporal evolution of the magma system. Historical eruptions, and especially the three most recent ones (occurred in 1951, 1995 and 2014–25), bring fluid inclusion evidence for transient, pre-eruptive shallow (9–17 km depth) magma ponding. Early post-collapse (60 ka) volcanics, in contrast, document fast magma transport from ~25 km, and suggest a reconfiguration of the magma system after the Monte Amarelo collapse event.

1. Introduction

Recent geophysical, mineralogical, and geochemical results have reshaped our understanding of the trans-crustal magmatic systems below active volcanoes. The emerging view of the subsurface structures of oceanic island volcanoes is that of complex, vertically extended magma systems with multiple levels of magma storage (e.g., Cashman and Giordano, 2014; Cashman et al., 2017; Cashman and Edmonds, 2019; Edmonds et al., 2019; Sparks et al., 2019). While thermal and rheological conditions in the lower crust favour melt segregation and fractionation, upper crustal magma systems are thought to take the form of non-eruptible mushes, separated by crystallised bodies and small magma lenses (Menand, 2011). This is remarkable in the case of shallow-level magma intrusions, such as those at oceanic island volcanoes (e.g., Schwarz et al., 2004; Klügel et al., 2005; Stroncik et al., 2009; Zanon et al., 2020). Under these circumstances, the lifetime of a magma system is strictly linked to magma supply rate and composition, and the stress field (Holtzman and Kohlstedt, 2007; Cooper and Kent, 2014; Parmigiani et al., 2014). In addition, the architecture of the magma system and ascent rates can vary from one eruption to another.

Understanding the architecture of a magma system is, therefore, key to modelling pre-eruptive storage conditions and ascent timescales (Cashman et al., 2017; Pappalardo and Buono, 2021), and it is of paramount importance for volcanic hazard assessment and risk mitigation. In the mush-dominated reservoir paradigm, geophysical methods and satellite-based observations may lack the required spatial resolution to identify melts stored in the crust (Foroozan et al., 2010; Mattioli et al., 2010; Voight et al., 2010; Biggs et al., 2014). Petrological methods, based on the post-hoc analysis of erupted rocks, are therefore invaluable in the definition of the pre-eruptive magma storage conditions and mechanisms/timescales of magma ascent. They can also probe the past temporal evolution of the plumbing system over the lifetime of the volcanic system. Fluid inclusions microthermometry is especially suited for this scope, as it provides information on pressure of fluid trapping and/or re-equilibration, which occurs during magma ponding, and hence the depths of pre-eruptive magma storage across multiple ponding

* Corresponding author.
E-mail address: Vittorio.VZ.Zanon@azores.gov.pt (V. Zanon).

https://doi.org/10.1016/j.jvolgeores.2022.107730
Received 6 June 2022; Received in revised form 20 November 2022; Accepted 1 December 2022
Available online 5 December 2022

levels (Hansteen et al., 1998). The concept of fluid inclusion assemblages (Goldstein et al., 2003) is useful, as it includes in the interpretation a large population of inclusions with the same composition, which have been trapped under the same environmental conditions. Interpreting single fluid inclusion might be biased by a complicated post-entrapment history.

In magmatic environments, fluid inclusions are bubbles of exsolved magmatic volatiles that are trapped in crystallographic defects during crystal growth, or during re-equilibration (Bodnar, 2003). Upon cooling, these fluids can undergo phase separation to vapour or liquid (Bodnar, 2003). The analysis of their composition and texture reveals different periods of formation and/or re-equilibration, which are barometrically constrained by the microthermometric study of phase changes of the fluid trapped.

Here, the fluid inclusion microthermometry has been used to characterise the crustal magma system of Fogo Volcano (Cape Verde Archipelago), one of the most frequently erupting intraplate volcanic systems on Earth (Siebert and Simkin, 2002). Previous petrological works (Hildner et al., 2011, 2012; Mata et al., 2017; Klügel et al., 2020) have used the fluid inclusions microthermometry and the clinopyroxene-melt barometry to the three most recent eruptions (1951, 1995 and 2014–15), but little information exists on the long-term stability or evolution of magma storage conditions. Our aim is to complement these previous studies by presenting new petrological, geochemical, and fluid inclusions results for lavas erupted during 11 eruptions spanning in age from ~120 ka to 2014–15. This temporal window encompasses the Monte Amarelo flank collapse, the major structural collapse event of the volcanic edifice. The architecture of the magma system of Fogo Volcano is re-evaluated through a fine-tuned study of fluid inclusions following the approach suggested by Zanon et al. (2020), that was applied to Pico Volcano in the Azores. This methodology combines the different densities (and, hence, entrapment pressures and depths) of fluid inclusion assemblages in the hosted phenocrysts to identify the different magma ponding levels during the magma ascent.

Our novel results provide new constraints on (i) the vertical arrangement of the plumbing system beneath Fogo Volcano (e.g., the different magma storage and stagnation levels, from the deep crust/upper mantle to the surface), and (ii) the temporal evolution of plumbing system in the last 120 thousand years.

2. Geological setting and volcanic history

The Cape Verde Archipelago (Fig. 1, inset), in the central Atlantic Ocean, stands on the Cape Verde Rise, the largest oceanic intraplate bathymetric anomaly on Earth (Wilson et al., 2013). The Cape Verde Rise marks an area of significant gravity, heat flow and anomalous seismic velocities at depth (Dash et al., 1976; Courtney and White, 1986; Wilson et al., 2013), interpreted as the surface expression of a hot-spot mantle swell (Liu and Zhao, 2014). Volcanism in the archipelago

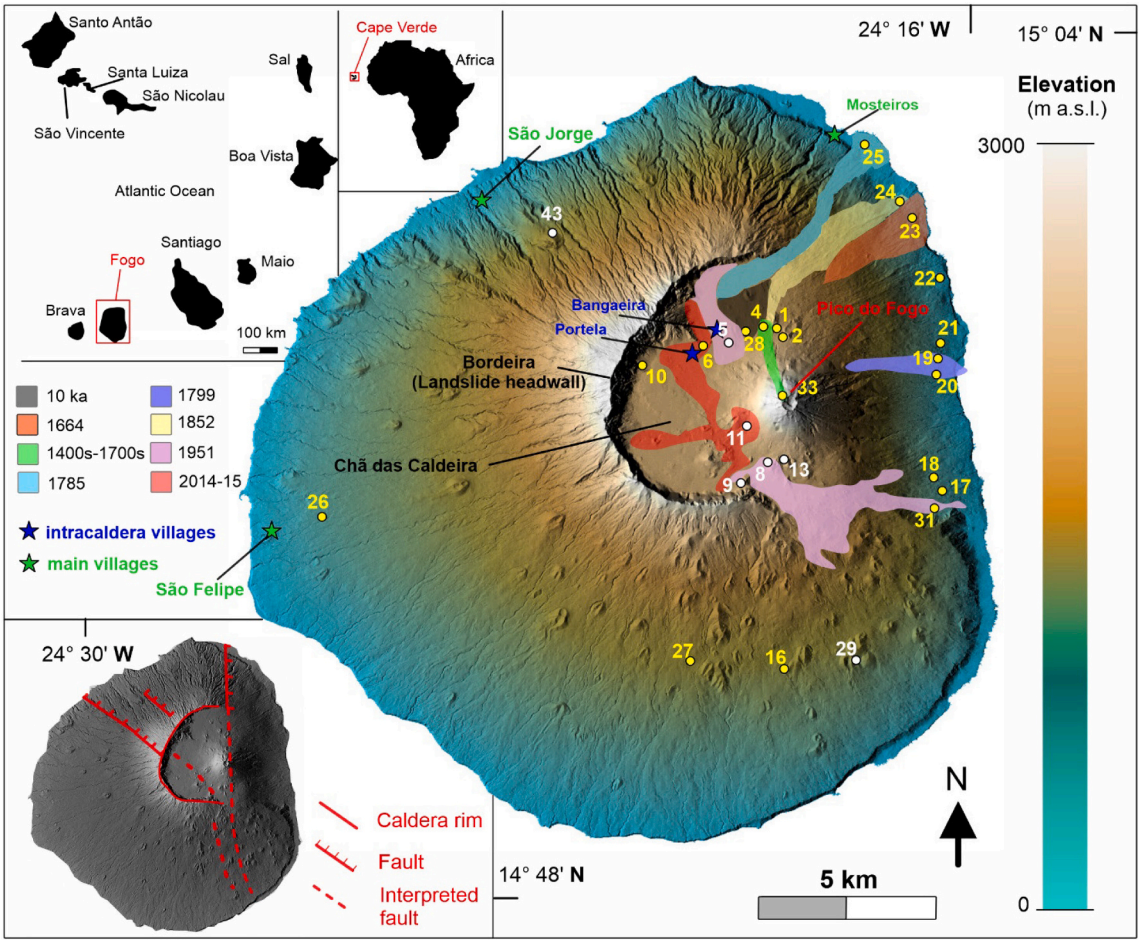

Fig. 1. Digital elevation map of Fogo Island (modified from: Official SketchFab internet site, managed by the Volcanology and Petrology lab's 3D models, Department of Geology and Geography, West Virginia University), showing lava sampling sites (yellow numbers) and tephra samples (white numbers). The studied eruptions are mapped from satellite images available from Google Earth, and existing geological maps (Torres et al., 1997; Carracedo et al., 2015). Insets show the position of the Cape Verde archipelago (top, right), and the Fogo Island (top, left) with the main fault systems (bottom, left) from literature (Day et al., 1999; Martínez-Moreno et al., 2018). (For interpretation of the references to colour in this figure legend, the reader is referred to the web version of this article.)

began ~26 Ma (Torres et al., 2010), and is dominated by silica-undersaturated melts of basanitic to phonolitic compositions (Gerlach et al., 1988), with rare carbonatites (Hoernle et al., 2002; Mourão et al., 2012).

Fogo Island (Fig. 1) formed and developed during the last 3–4.5 Ma, and has been the only site of volcanism since the first historical report in the 15th century, with at least 28 recorded eruptions (Ribeiro, 1954; Torres et al., 1997). Historic activity concentrated on and around Pico do Fogo (Fig. 1), a steep cone formed inside Chã das Caldeira, a ~ 8 km wide semi-circular depression resulting from the flank collapse event of the Monte Amarelo Volcano, which has been dated at ~73 ka (Day et al., 1999) to 62–123 ka (Foeken et al., 2009). The volcanological evolution of Fogo includes four eruptive phases:

1. the Ribeira de Almada Group: carbonatitic and alkali-rick mafic submarine lavas dated at ~4.5 Ma (Foeken et al., 2007, 2009);
2. the Monte Barro Group: the first sub-aerial lavas of unknown age;
3. the Monte Amarelo Group (no absolute chronology): a ~ 2–3 km thick succession of alkaline mafic to intermediate lavas, emplaced before the lateral collapse of the volcano;
4. the Chã das Caldeira Group: the youngest eruptive phase, subdivided into the Pico do Fogo and Monte Orlando formations (Foeken et al., 2009). The former includes the volcanic products emplaced during protracted summit/central activity at Pico do Fogo, in between the Monte Amarelo collapse and the 1785 eruption (Ribeiro, 1954). The Monte Orlando formation includes fissure-fed effusive eruptions concentrating along the Pico do Fogo flanks, from the 18th century onward (Day et al., 2000). These eruptions clustered along N-S trending fissures/fractures, except for the 1995 and 2014–15 eruptions, that occurred on Pico do Fogo's south-western flank.

3. Materials and methods

Twenty-seven rock samples spanning the last 120 ka of volcanic activity were studied (Fig. 1, Supplementary Data Table 1). Five of them are extra-caldera lavas and proximal tephra fall deposits with ages from ~120 to ~10 ka (Foeken et al., 2009; Carracedo et al., 2015), and 22 are Holocene/historical intra-caldera samples (17 lava flows and 5 tephra deposits).

Whole-rock major element compositions were measured in 21 samples (Supplementary data 2) with a Perkin Elmer 9000 inductively coupled plasma-mass spectrometer (ICP-MS) at Activation Laboratories (Actlabs), Ontario, Canada. Alkaline dissolution with lithium metaborate/tetraborate, followed by nitric acid, was used on 1 g of rock powders before fusion in an induction furnace. The melt was poured into a solution of 5% nitric acid containing cadmium as an internal standard and stirred until complete dissolution. The analytical precision is better than 5% for all major elements.

Petrographic study and modal analysis were conducted on 21 thin sections, representative for 16 eruptions (Supplementary data 3) with a semi-automated digital point counter at the Instituto de Investigação em Vulcanologia e Avaliação de Riscos (IVAR), Ponta Delgada, Portugal.

For the study of fluid inclusions assemblages (FIAs), rocks were coarsely crushed and then sieved to separate grain size populations in the 250–4000 μm range. For each sample, about 200 olivine and 200 clinopyroxene phenocrysts were hand-picked from the grain size fractions. Crystals were doubly polished with silica carbide paper and alumina to attain a maximum thickness of 80–100 μm for olivine and 60–70 μm for pyroxenes. About 0.7% of investigated olivine and 0.3% of clinopyroxene contain FIAs, these were separated for a micro-textural study, inclusions mapping and microthermometry analysis.

Electron microprobe analyses on olivine and pyroxene crystals and groundmass were carried at the CAMPARIS centre (University of Paris La Sorbonne, France), using a CAMECA SX-Five electron microprobe, equipped with five WDS spectrometers and an EDS detector. Seventeen olivine crystals, 14 pyroxenes crystals and 16 fragments of groundmass were analysed, with a 15-kV accelerating voltage and a 20 nA current beam, with counting times from 10 to 20 s on the peak. We checked the accuracy against the San Carlos Olivine international standard. The relative errors are <6.5% for Ni and Mn, <5% for Fe and Ca, and < 1% for Si and Mg.

Two olivine and two clinopyroxene compositional data (Supplementary data 4) coupled with groundmass electron microprobe analysis were used to estimate the magma temperature by applying the olivine-liquid geothermobarometer of Putirka et al. (2007) (eq. 4) and the clinopyroxene-liquid geothermobarometer of Putirka (2008) (eq. 33). We tested the chemical equilibrium hypothesis using the Rhodes diagram (Rhodes et al., 1979) and the observed (Kd $(Fe\text{-}Mg)_{ol\text{-}liq} = 0.26 \pm 0.02$; Kd $(Fe\text{-}Mg)_{cpx\text{-}liq} = 0.27 \pm 0.01$) and equilibrium (Kd $(Fe\text{-}Mg)_{cpx/olv\text{-}liq} = 0.27 \pm 0.03$) Fe-Mg exchange coefficients were in close agreement.

Microthermometry data were measured on 2691 inclusions (from a selection of 15 samples from 11 eruptions; Table 1) using a Linkam MDSG600 heating-cooling stage, at the Instituto de Investigação em Vulcanologia e Avaliação de Riscos (IVAR), Ponta Delgada, Portugal. The stage was calibrated using synthetic fluid inclusions of pure CO_2 and H_2O. A heating rate of 0.2–0.5 °C/min was used, resulting in a ± 0.1 °C accuracy during melting and homogenisation. Density values for pure-CO_2 fluid inclusions were derived from measured homogenisation temperatures (Th) using eqs. 3.14 and 3.15 in Span and Wagner (1996). The equation of Sterner and Bodnar (1991) was used to calculate the densities of fluid inclusions, after the correction suggested by Hansteen and Klugel (2008) that accounts for the pristine presence of a maximum 10% molar volume of H_2O in the fluid inclusions during their formation (CO_2:H_2O ratios of 9:1). We use this correction to account for the fact that, at the time of trapping, the fluid may also have contained some H_2O (Hansteen and Klugel, 2008). This water was the lost upon cooling by diffusion (Barth et al., 2019; Frezzotti et al., 2012). Previous work in intraplate magmatism context (Dixon and Stolper, 1995; Hansteen and Klugel, 2008) supports this 10 mol% H_2O upper limit for the FIAs trapped at upper mantle conditions.

Isochores, which are based on fluid density and composition, and hosted mineral composition, allows the derivation of fluid trapping pressure at assumed or calculated temperature. The FLUIDS software (Bakker, 2003) was used for isochores calculation.

4. Results

All studied samples are nepheline-normative (8.4–25.4%) basanites (SiO_2 = 41.08–44.26 wt%; $K_2O + Na_2O$ = 2.99–9.35 wt%), forming an evolution trend towards the foidite field in the TAS diagram (Fig. 2a). A single lava contains up to 45 vol% of mafic phenocrysts as cumulate phases and, therefore, plot close to the boundary with picrites (SiO_2 = 41.53 wt%; $K_2O + Na_2O$ = 2.99 wt%).

Basanites are porphyritic (vesicle-free, average 67.8 vol% phenocrysts), with the common mineral assemblage represented by clinopyroxene, olivine, plagioclase, and Fe-Ti oxides. Amphibole is rare, but it is present in the last three eruptions and has decomposition rims of variable thickness (from 100 μm to amphibole total decomposition). The microcrystalline groundmass (<50 μm) is intergranular and is made up of dominant plagioclase and lesser olivine and clinopyroxene. The two alkali-rich lavas are poorly porphyritic (13.3 and 4.1 vol%), with micro phenocrysts (in the 50–500 μm size range) of clinopyroxene, olivine, plagioclase, and Fe-Ti oxide. The crystal-rich lava (vesicle-free,~ 37.3 vol % phenocrysts) is characterised by 10.8 vol% clinopyroxene phenocrysts that occur as pinkish, Ti-rich, patchy zoned phenocrysts (and pale green phenocrysts), set in a groundmass of plagioclase, olivine, and Fe-Ti oxides.

The studied clinopyroxene are diopsides (Wo_{49} En_{32} Fs_{11} to Wo_{52} En_{40} Fs_{15}) except a single augite crystal (Wo_{33} En_{42} Fs_{26}) (Fig. 2b). Clinopyroxene phenocrysts show a wide Al_2O_3 range (5.64–14.19 wt%), while TiO_2 (2.44–5.89 wt%) and Na_2O (0.37–2.38 wt%) are less

Table 1
Summary of microthermometry results for FIAs in olivine (top) and clinopyroxene (bottom). Owing to the large microthermometric dataset, results are presented as ranges for individual eruptions, rather than data for individual inclusions. The calculation of isochores used magmatic temperatures of 1133 °C and 1134 °C from clinopyroxene and olivine thermometry respectively. Corresponding depths are derived using a reference crustal model (see text). Uncertainties on individual calculations of densities are ±1 kg·m^{-3}, for Th < 25 °C and ± 2 kg·m^{-3}, for Th >25 °C. Whereas for the derived pressures, uncertainties are ±5–8 MPa, for fluid densities in the 500–700 kg·m^{-3} range and ± 8–15 MPa in the 700 to 900 kg·m^{-3} density range.

Olivine

Sample ID	Eruption	Number of analysed crystals	Number of measurements	Homogenisation temperature Th_L (°C)	Density (kg·m^{-3})		Density H_2O-corrected (kg·m^{-3})		Pressure (Mpa)	Depth (km)
					Type I	*Type II*	*Type I*	*Type II*		
Fog 26	120 ka	2	85	15.6–22.6	744–814	/	778–853	/	497–595	16.2–19.5
Fog 27	60 ka	3	73	2.8–3.7	904–910	/	946–952	/	700–740	23.0–24.3
Fog 28	10 ka intracaldera	2	125	21.6–27.1	675–755	/	706–790	/	405–510	13.1–16.7
Fog 43	10 ka extracaldera	2	198	13.4–30.8	802–835	537–651	839–873	561–680	260–625	9.8–20.5
Fog 23	1664	3	238	11.9–20.6	767–847	/	802–886	/	540–640	17.7–21.0
Fog 4, 33	1400s–1700s	5	370	16.5–23.1	672–808	659–665	702–845	689–696	390–585	12.8–19.2
Fog 25	1785	1	20	29.9–30.9	/	520–600	/	543–627	245–315	9.2–10.3
Fog 19, 20	1799	7	191	18.8–30.8	667–787	596–659	698–822	623–689	311–554	11.7–18.2
Fog 24	1852	2	61	15.2–29.9	799–825	598–668	836–863	625–699	315–600	11.8–19.7
Fog 5,8,31	1951	7	587	21.9–30.8	656–753	537–647	686–787	561–676	305–510	11.5–16.7
Fog 11	2014–15	2	169	26.6–30.2	663–689	586–647	693–721	613–676	305–425	11.5–13.9

Clinopyroxene

Sample ID	eruption	Number of analysed crystals	Number of measurements	Homogenisation temperature Th_L (°C)	Density H_2O-uncorrected (kg·m^{-3})		Density H_2O-corrected (kg·m^{-3})		Pressure (Mpa)	Depth (km)
					Type I	*Type II*	*Type I*	*Type II*		
Fog 23	1664	2	55	26.9–29.5	672–679	615–647	703–710	643–676	340–420	11.9–14.7
Fog 4,33	1400s–1700s	2	90	30.2–30.7	/	554–583	/	579–610	280–308	9.8–10.8
Fog 25	1785	3	177	29.6–30.2	/	583–611	/	610–639	308–340	10.8–11.9
Fog 19,20	1799	2	151	28.8–30.8	/	537–636	/	561–665	265–366	9.3–12.8
Fog 5, 31	1951	2	188	29.8–30.9	/	520–604	/	543–631	248–330	8.7–11.5

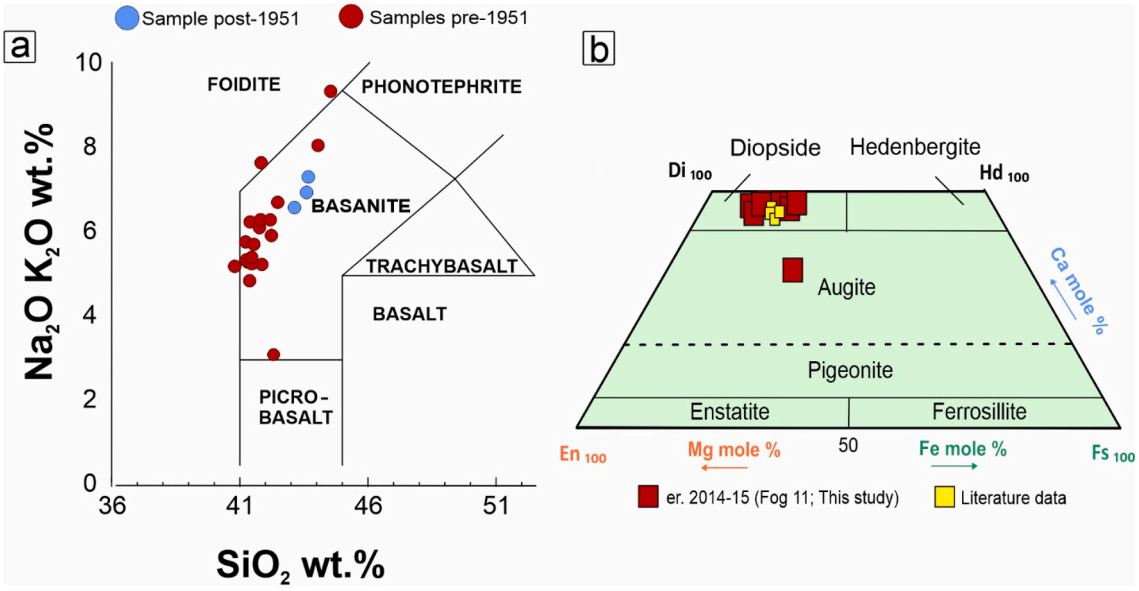

Fig. 2. Total alkali-silica (TAS) diagram (a) and pyroxene quadrilateral classification (b). Literature data are from Mata et al. (2017). All pyroxene analyses were conducted on sample Fog 11 from the 2014–2015 eruption.

variable. The Mg# ranges from 62 to 79. Olivine phenocrysts have forsterite contents ranging from Fo_{77} to Fo_{84}, low CaO (0.28–0.38 wt%), and NiO in the range 0.04–0.13 wt%, (Supplementary data 4).

4.1. Petrography of FIAs

Both olivine and pyroxene phenocrysts trapped FIAs, while megacrysts (> 1000 μm) are devoid. Fluid inclusion diameters are variable (up to 41 μm) and around 5–10 μm. Below the temperature of homogenisation (Th = 2.8–30.8 °C) all fluid inclusions are two-phase (L + V), with liquid volume being more abundant than vapour. Fluid inclusions do not contain visible daughter minerals or co-trapped minerals.

Shapes range from negative-crystal to elliptic as a function of their formation dynamics; the early-stage fluid inclusions, entrapped during crystal formation and growth, exhibit rounded/semi-rounded shapes, whereas late-stage inclusions, which result from re-equilibration processes of the fluid, have elliptic shapes. Here, we follow the textural criteria in Zanon and Frezzotti (2013) to distinguish between early (Type I) and late (Type II) stage inclusions. Type I inclusions (Fig. 3a) are isolated or occur in small clusters, and their texture shows no evidence of decrepitation. Type II inclusions (Fig. 3b) are present in linear trails along healed fractures and have likely experienced volume stretching and/or leaking. Evidence of partial or total density re-equilibration includes a visible black border surrounding the inclusions, and radial short cracks, generated by decrepitation near the inclusion (Fig. 3c). Type II fluid inclusions are more abundant, with Type II to Type I proportion of about 4:1 in olivine phenocrysts and 5:1 in clinopyroxene phenocrysts.

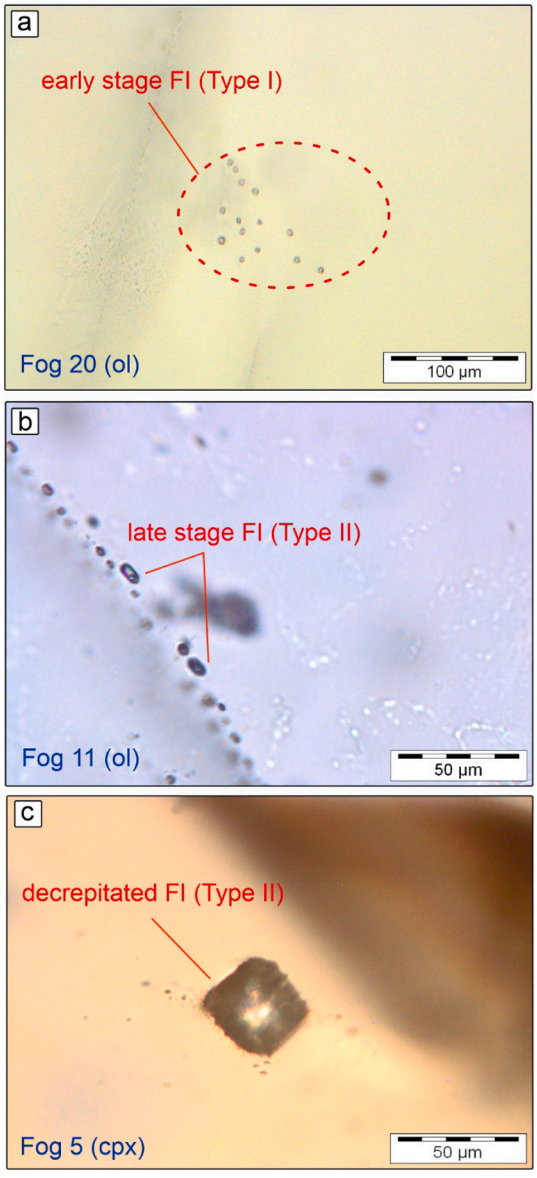

Fig. 3. Photomicrographs of texturally different fluid inclusions hosted in olivine and clinopyroxene. (a) Cluster of Type I rounded fluid inclusions. (b) Type II elliptic fluid inclusions along trails. (c) Isolated decrepitated fluid inclusion with squared/irregular shape, surrounded by visible microfractures.

4.2. Microthermometry of FIAs

About 2700 fluid inclusions (an average of 68 fluid inclusions for each olivine and 51 for each clinopyroxene), hosted in 36 olivines and 11 clinopyroxenes, were analysed. On cooling, nearly all inclusions froze between −80 and −105 °C, and melted at $T_m = -56.6 \pm 0.1$ °C, which characterises a pure CO_2 fluid composition (Wilmart et al., 1991). Upon heating, inclusions homogenized to the liquid phase in a range of temperatures (Th_L) from 2.8 to 30.8 °C, corresponding to densities between 952 and 543 kg·m^{-3} (uncertainty in density calculation, is on average 5.0%). No inclusion homogenising to the vapour phase has been found, showing a lack of low CO_2 density inclusions. 136 inclusions in two olivines from sample Fog 20, melted between −58.1 and −56.8 °C, showing micromole amounts of other volatile species. These inclusions homogenized to a liquid phase in the range 19.2 to 20.3 °C and represent only a small (<5%) fraction of the analysed inclusions; for this reason, they will not be further considered.

Table 1 lists both raw (uncorrected for H_2O content) and H_2O-corrected density values. We report density ranges for individual eruptions, noting that values measured within individual mineral grains vary within a narrow range (± 5.0% of the average), implying homogeneous trapping histories. The analysed samples cover a prolonged temporal interval of volcanic activity that encompasses the Monte Amarelo collapse. This event marks a major turning point in the morphological evolution of Fogo Island; therefore, the following description will follow a temporal sequence, corroborated by the histograms of density distribution of Fig. 4.

Pre-collapse period sample (120 ka) - Fog 26 is the only sample representative of volcanic activity before the Monte Amarelo collapse. The derived fluid inclusion densities for this eruption, as inferred from the analysis of Type I inclusions only, show a bimodal distribution, with H_2O-corrected densities ranging from 778 to 853 kg·m^{-3}.

Early post-collapse phase sample (60 ka) – The sample Fog 27 represents volcanic activity after the Monte Amarelo collapse. Type I inclusions show a unimodal distribution of densities (ranging from 946 to 952 kg·m^{-3}).

Holocene/historical eruptions (10 ka – 2014/15) - The density populations show polymodal and skewed distributions. Olivine and clinopyroxene trap both Type I and Type II inclusions. Densities of Type I inclusions in olivine range from as low as 686 kg·m^{-3} (1951 eruption) to as high as 886 kg·m^{-3} (1664 eruption). Type I inclusions are present in clinopyroxene from only a single sample (Fog 23; 1664 eruption) and inclusion densities are 703–710 kg·m^{-3}. Type II inclusions show densities ranging from 543 to 699 kg·m^{-3} in olivine and from 543 to 676 kg·m^{-3} in clinopyroxene.

5. Discussion

5.1. Interpretation of histograms of FIAs density populations

The frequency distribution of inclusion densities, as recorded in crystals of each eruption, reflects the conditions of magma storage/ascent before that specific event (Zanon and Frezzotti, 2013).

We have identified two texturally distinct FIAs Types (Fig. 3).

Rounded/semi-rounded, isolated Type I FIAs (Fig. 3) are interpreted (Bodnar, 2003; Zanon and Frezzotti, 2013) to form in response to slow

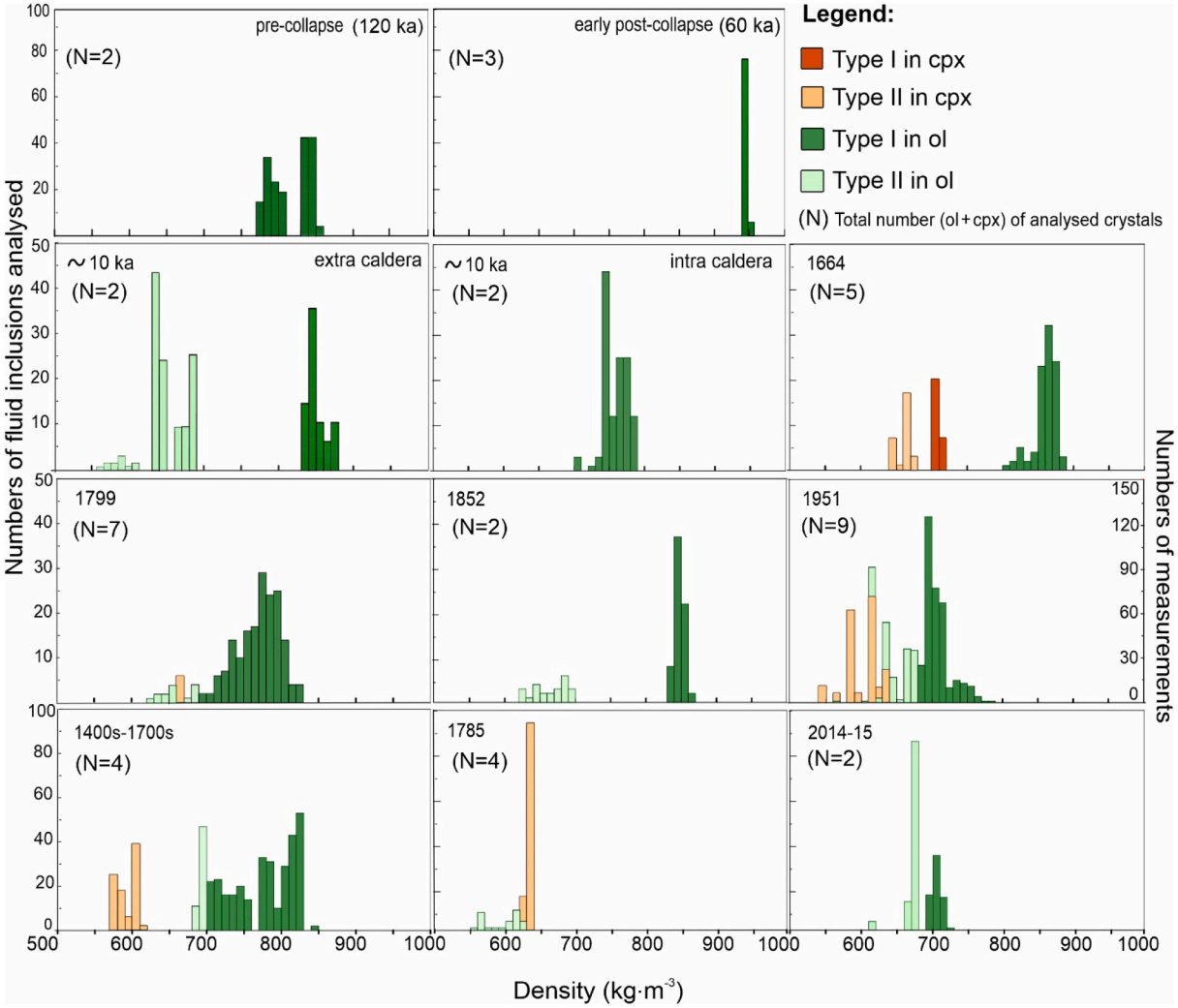

Fig. 4. Histograms of fluid inclusion densities (H_2O-corrected) for the eruptions studied. Barometric results for olivine-hosted fluid inclusions (dark green: Type I; light green: Type II) and clinopyroxene-hosted fluid inclusions (red: Type I; orange: Type II) are shown. These histograms show variable density frequency distributions, ranging from sharp and unimodal (e.g., the ~60 ka early post-collapse eruption) to complex and polymodal (e.g., pre-collapse, ~120 ka), implying distinct conditions of magma storage and ascent. The highest density values are observed for the Monte Amarelo post-collapse eruption (~60 ka) and the lowest for Fogo's most recent eruption (2014–15). (For interpretation of the references to colour in this figure legend, the reader is referred to the web version of this article.)

crystal growth during magma storage. The modern paradigm of vertically extended magma systems (Cashman et al., 2017) imposes a heterogeneous distribution of gas bubbles and of (different populations of) crystals in a magma storage zone. A magma system can be fluxed by CO_2-rich fluids released from a deep source (Caricchi et al., 2018) which could be responsible for fluid inclusions formation. Since gas bubbles are likely to distribute heterogeneously (and accumulate at local geometrical/rheological discontinuities; Edmonds et al., 2019), Type I FIAs are hence expected to be entrapped over a range of P-T-X conditions. This is because magma slowly rises through the multiple (staked) magma lenses that make a vertically extended magma system, Type I FIAs can undergo re-equilibration (to lower densities) because of decompression, generating internal fluid overpressure (non-isochoric ascent path; (Frezzotti and Peccerillo, 2004). During prolonged magma ponding, this re-equilibration process involves all the FIAs which are now reset to the new pressure conditions of the shallower magma storage zone, thus loosing memory of deeper entrapment conditions. Ultimately, several distinct populations of Type I FIAs can be found in different mineral grains of a sample, whose density distributions reflect the multiple, over-imposed regions of magma storage. The depth interval recorded by each Type I FIA populations has a geo-volcanological meaning (e.g., it corresponds to specific level of transient magma storage) if it is recurrently observed in several eruptions.

The second typology of FIAs – Type II – are texturally identified as trails of inclusions aligned along crystal fractures. At Fogo, these Type II FIAs record lower densities (Fig. 4). They therefore form upon further magma ascent and decompression, as large fluid overpressure develops in Type I inclusions, causing them to decrepitate and fail. Healing of micro cracks caused by fluid overpressure during magma decompression is, therefore, the dominant mode of Type II fluid inclusion formation (Roedder, 1984). Crystal fracturing/regrowth during decompression-driven magma ascent and degassing, and/or during magma mixing, contribute to Type II FIA formation.

The ultimate effect of the multiple events of fluid redistribution (described above) is the generation of several FIA populations, as evidenced by complex polymodal density curves (Fig. 4). Joint interpretation of a set of polymodal density distributions, obtained for several eruptions which occurred over short activity periods (Fig. 4), offer the opportunity to identify geological discontinuities at depth (Zanon et al., 2020).

The density distributions for the Fogo eruptions studied are variable, and range from (i) sharp, narrow, and unimodal (e.g., ~60 ka eruption), to (ii) broad, skewed, and unimodal (e.g., 1799 eruption), and (iii) complex and polymodal (e.g., ~120 ka eruption). These observations

suggest that the conditions of magma storage, and the rates and modes of magma ascent (that control FIAs re-equilibration), are distinct for each eruption. Overall, the highest density values are observed for the early post-collapse (~60 ka) eruption (Fog 27; 946–952 kg·m^{-3}), and lowest for the 2014–15 eruption (693–721 kg·m^{-3}).

We find that the densities of FIAs trapped in clinopyroxene are always lower than in olivine. This is consistent with the common observation (Hansteen et al., 1998; Galipp et al., 2006) that FIAs in clinopyroxene undergo faster re-equilibration (than olivine), because of the presence of two planes of cleavage. We cannot exclude, however, that the lower densities recorded by FIAs in clinopyroxene just reflect a late (and shallower) crystallization of this mineral phase. The only exception is represented by the 1785 eruption, whose lavas carry frequent but fluid inclusion-free olivine.

5.2. Entrapment pressures and depths

The H_2O-corrected densities have been converted into pressures (Table 1) of inclusion entrapment and/or re-equilibration (Fig. 5) from isochore calculations at the temperature of olivine and pyroxene crystallization. These temperatures have been obtained using the olivine-liquid and clinopyroxene-liquid geothermometers (Putirka, 2008, eq. 33 and Putirka et al., 2007, eq. 21). The two geothermometers provide the same temperature ranges (i.e., 1133 ± 26 °C for the clinopyroxene-melt and 1134 ± 10 °C for the olivine-melt geothermobarometer). We note that uncertainties on temperature estimation have a minor influence on calculated pressures: a ± 20 °C temperature uncertainty converts into 1–2% change in calculated fluid inclusion pressures.

Converting pressures into depths (Table 1) requires a reference model for the crustal structure, including the location of the upper mantle-crust transition underneath the volcano. Here, interpreting geophysical data generated contrasting models. Large changes in V_P/V_S have been recognized at depths of 12 ± 1 km (Vinnik et al., 2012; Pim et al., 2008; Wilson et al., 2013) and 30 km (Vinnik et al., 2012). Basing upon these depths, it is possible to hypothesize that the first 12 km consists of lavas and small intrusive bodies being part of the oceanic crust with a density of 2700 kg·m^{-3} (Carlson and Raskin, 1984). The rocks up to 30 km depth should be part of the deeper magma system of the volcano, formed by ultramafic cumulates, crystal mushes and/or mantle lithologies (Cooper et al., 1992; Tenzer et al., 2013). For these rocks, a general density of 3100 kg·m^{-3} was assumed.The Fig. 5 shows the resulting pressure estimates. Entrapment pressures from 248 to 740 MPa suggest that Fogo magmas coexist with a CO_2-dominated fluid phase throughout their entire ascent path, in agreement with the low CO_2 solubility in silicate melts (Métrich and Wallace, 2008). There is a good matching with literature data for the last three eruptions for the shallow magma systems (Fig. 5). However, there is also a deep level of entrapment of FIAs (>500 MPa), providing independent support for a deep magma storage zone (at 17–25 km) that had so far been only identified by cpx-melt geothermobarometry (Hildner et al., 2011, 2012; Klügel et al., 2020).

The following paragraphs describe the distinct entrapment conditions for pre-collapse, early post-collapse, and Holocene/historical eruptions.

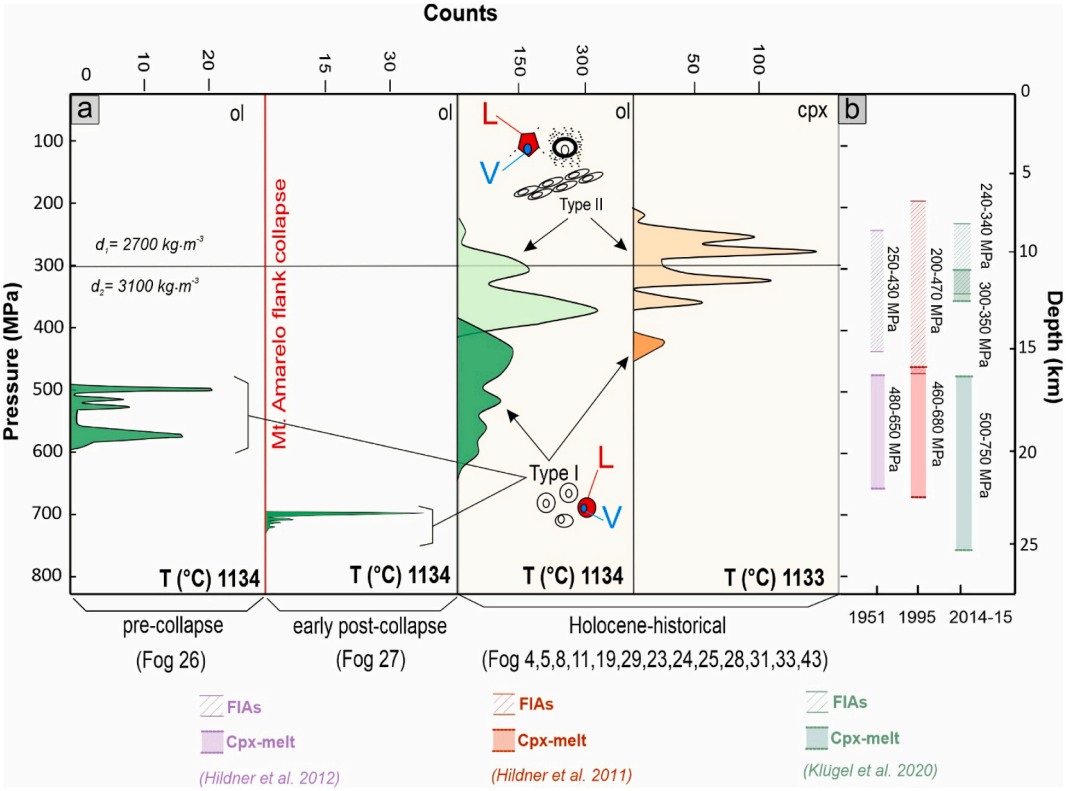

Fig. 5. (a) FIAs entrapment/re-equilibration pressures (and corresponding depths). (left), pre-collapse eruption; (centre), early post-collapse eruption; (right) Holocene/historical eruptions (green, olivine-hosted; orange, clinopyroxene-hosted; dark tones, Type I fluid inclusions; light tones, Type II fluid inclusions; schematic representations of Type I and Type II fluid inclusions, in both the two different fluid phases (Liquid, L and Vapour, V) are signed by red (L) and light blue (V) colours). The melt temperatures are derived with different geothermobarometers (see text) and are used to convert density values in trapping pressures. The highest pressures are recorded in an early post-collapse eruption (~60 ka). Type II fluid inclusions identify a low-pressure region where magma ponded for a short time and where inclusions re-equilibrated before the final ascent to the surface. The thin horizontal black line shows the boundary between two layers of the stratigraphic model underneath Fogo (see text) characterised by different densities (d_1 and d_2). (b) Comparison with literature data (Hildner et al., 2011, 2012; Klügel et al., 2020). (For interpretation of the references to colour in this figure legend, the reader is referred to the web version of this article.)

5.2.1. Pre-collapse phase (~120 ka eruption)

There are two FIAs entrapment pressure intervals at 557–595 MPa and 497–529 MPa, corresponding to olivine growth. These data therefore show magma storage areas at depths of ~19 ± 0.9 km and ~ 17 ± 0.7 km. These depths match the shallowest to intermediate portions of the 17–25 km deep magma storage zone identified in the literature. There is no evidence FIAs entrapment/re-equilibration at depths <17 km, suggesting a rapid magma ascent through the upper crust.

5.2.2. Early post-collapse phase (~60 ka eruption)

The FIAs in olivine record entrapment pressures from 700 to 740 MPa, the deepest so far obtained for this volcano using fluid inclusions. These correspond to inferred entrapment depths of 23.7 ± 0.9 km, and therefore to the roots of the 17–25 km deep magma storage zone already identified in literature.

5.2.3. Holocene/historical activity (≤ 10 ka to 2014–2015 eruption)

The FIAs in olivine record a range of entrapment pressures from 245 to 640 MPa which are lower than those of the early post-collapse (Fig. 5). Type I FiAs provided entrapment pressures between 384 and 640 MPa, suggesting that these recent eruptions have been fed by magma which ascended from a depth of ~13 to ~21 km. Type II FIAs in clinopyroxene (Fig. 5) record shallower entrapment conditions of 248 to 380 MPa, corresponding to depths from 9.4 to 12.5 km.

5.3. Temporal evolution of the magma plumbing system

These results contribute to refine the view of the architecture of the magma system underneath Fogo Volcano. This large fluid inclusion dataset can help to better understand if, and to what extent, such conditions of pre-eruptive magma storage and ascent have evolved through time at this volcano.

Some FIAs entrapment pressure/depth intervals recur in distinct eruptions spanning thousands of years (Fig. 6). These depth intervals are interpreted as magma accumulation zones, which are stable through time. The deepest of these magma storage regions (23.7 ± 0.9 km) is only recorded by the olivine-hosted FIAs in the ~60 ka early post-collapse lavas. The difference with the pre-collapse lava sample suggests some re-organisation of the magma system after the Monte Amarelo collapse event, as previously found (Hildner et al., 2012). We

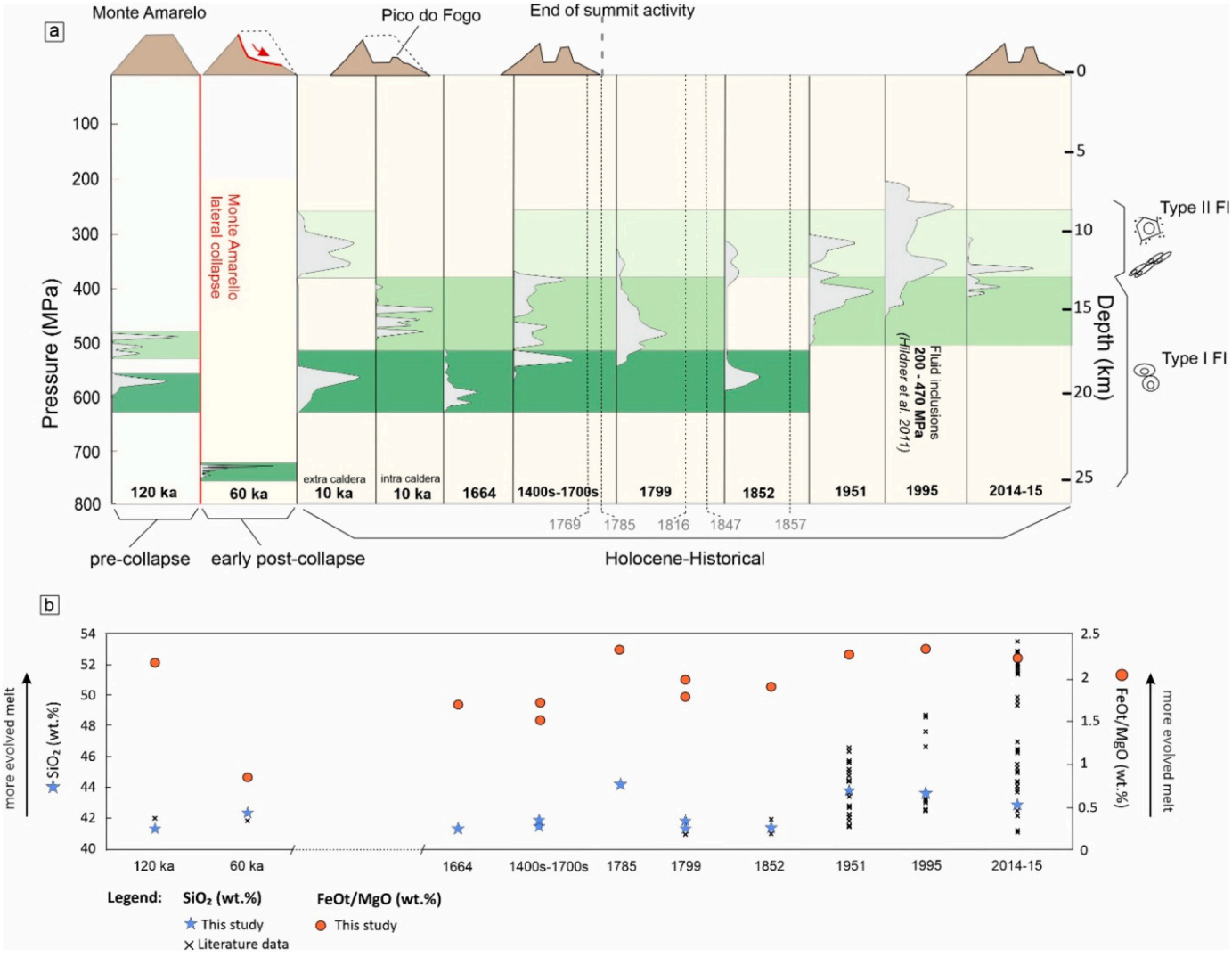

Fig. 6. (a) Temporal evolution of entrapment/re-equilibration pressures/depths for the studied Fogo eruptions, based on FIAs in olivine phenocrysts only. The coloured bands mark regions of magma ponding that recur in several eruptions. Key-magma storage areas are observed at ~22–25 km, ~19 km and ~ 15–17 km. Type II inclusions show FIAs re-equilibrations at ~9–12 km. Low-density inclusions (of both types) suggest that deep crustal (9–17 km) magma ponding has been recurrent in historical time, and especially before the 1951, 1995 and 2014–2015 eruptions, during which more evolved lavas have been erupted, as shown by (b), temporal plots of bulk-rock SiO_2 contents and FeO_t/MgO ratios in the studied eruptions (data from the Hildner et al., 2011, 2012; Magnusson, 2016; Mata et al., 2017 and from this study, Table A1). Grey numbers mark the dates of non-studied eruptions.

argue that the formation of deep faults, as commonly observed in response to lateral collapse events (Amelung and Day, 2002), may have contributed to a fast withdrawal of deeply stored magmas. Rapid magma ascent (besides the disruption of any existing shallow magma reservoirs) would have reduced the possibility for further FIAs entrapment/re-equilibration, ultimately determining the absence of shallow pressure records in fluid inclusions for this eruption (Fig. 6). Post-collapse re-activation of deep reservoirs is indeed not unique to Fogo, but rather a recurrent feature at other oceanic volcanoes, such as El Hierro (Carracedo, 1999; Manconi et al., 2009) and La Palma (Galipp et al., 2006), the Canary Islands, and Piton de la Fournaise at La Reunion Island (Lénat and Bàchelery, 1990). The lack of lower pressure entrapment conditions in the FOG 27 olivine confirms little or no shallow crustal processing/stalling of magma in the early post-collapse phase (at ~60 ka eruption). This contrasts with the more recent historical eruptions that have more shallow crustal stalling/processing (see below).

Type I inclusions in olivine from the pre-collapse eruption and from Holocene/historical eruptions identify two major magma ponding regions (dark to light-dark green areas in Fig. 6) in the ~13 to ~19 km depth interval. The deepest level (dark green) is recorded in the Monte Amarelo products and in four Holocene/historical eruptions. The shallower ponding region begins at a depth of ~17 ± 0.7 km for the eruption of 120 ka; at ~15.5 ± 2.9 km depth in Holocene/historical eruptions (~10 ka intra caldera, 1400s–1700s, and 1799); and at ~15 ± 2.4 km depth in the 1951 and 2014–15 eruptions. This latter depth (~14 ± 0.3 km) is also shown by data in clinopyroxene phenocrysts. These two regions are interpreted as portions of a vertically extended magma system, in which multiple, distinct magma ponding zones exist that are repeatedly tapped/re-activated during individual eruptions (Fig. 7). As clinopyroxene-melt geothermobarometry shows a deeper (17–25 km) source for the most recent historical eruptions, these levels from ~13 to ~19 km should be interpreted as intermediate regions where magmas undergo prolonged ponding, crystallization and degassing, thus entrapping fluid inclusions in a exsolved fluid-rich magmatic environment. We cannot exclude that deeply formed (> 21 km) fluid inclusions exist whose density resets to lower values during decompression/temporal storage in the ~13–19 km depth range. Notably, these magma processes, absent in the early post-collapse ~60 ka eruption, have been at work since ~10 ka at least, and have remained a recurrent feature of Fogo activity from there onward.

Type II inclusions, both in olivine and clinopyroxene phenocrysts in all Holocene/historical eruptions, record depths of 9–12 km (light green in Fig. 6). We interpret this region as a portion of the magma system where the originally trapped fluid inclusions (Type I) undergo density re-equilibration, leading to fluid redistribution along crystal fracturs, ultimately forming trails of (Type II) fluid inclusions. There are multiple causes that can determine such re-equilibration, including crystal fracturing and re-growth driven by de-compressional degassing during magma ascent, and/or by mixing of chemically/thermally distinct magma batches/lenses (Neave et al., 2021). Ultimately, re-equilibration takes place in response to crystals experiencing (upon ascent) lower external pressures relative to the initial fluid internal isochoric conditions (Frezzotti et al., 2012). Whatever the cause, the presence of Type II FIAs in Holocene/historical eruptions – and their absence in older ones - reflects slower magma ascent rates, as longer residence times in the 9–12 km region are necessary for inclusion re-equilibration to occur (Zanon et al., 2020). At the very end of the spectrum of possible processes, formation of Type II FIAs may reflect short-lived stagnation events at 9–12 km depth taking place during magma ascent. In any case, our results would suggest that the growth of the Pico do Fogo cone, during protracted historical activity, has been associated with less direct ascent from the deep- to mid-crust than in the early post-collapse phase. There is no evidence for magma stagnation at depths <9 km (Figs. 5, 6), excluding any role played by shallow sin-eruptive magmatic processes in FIAs re-equilibration.

Overall, the 1951, 1995 and 2014–2015 eruptions show an apparent upward migration of magma storage regions (Fig. 6). These eruptions additionally show more prolonged re-equilibration events at <12 km than in other analysed samples (as shown by the abundant Type II inclusions). Assuming, from literature data (Klügel et al., 2020), that the

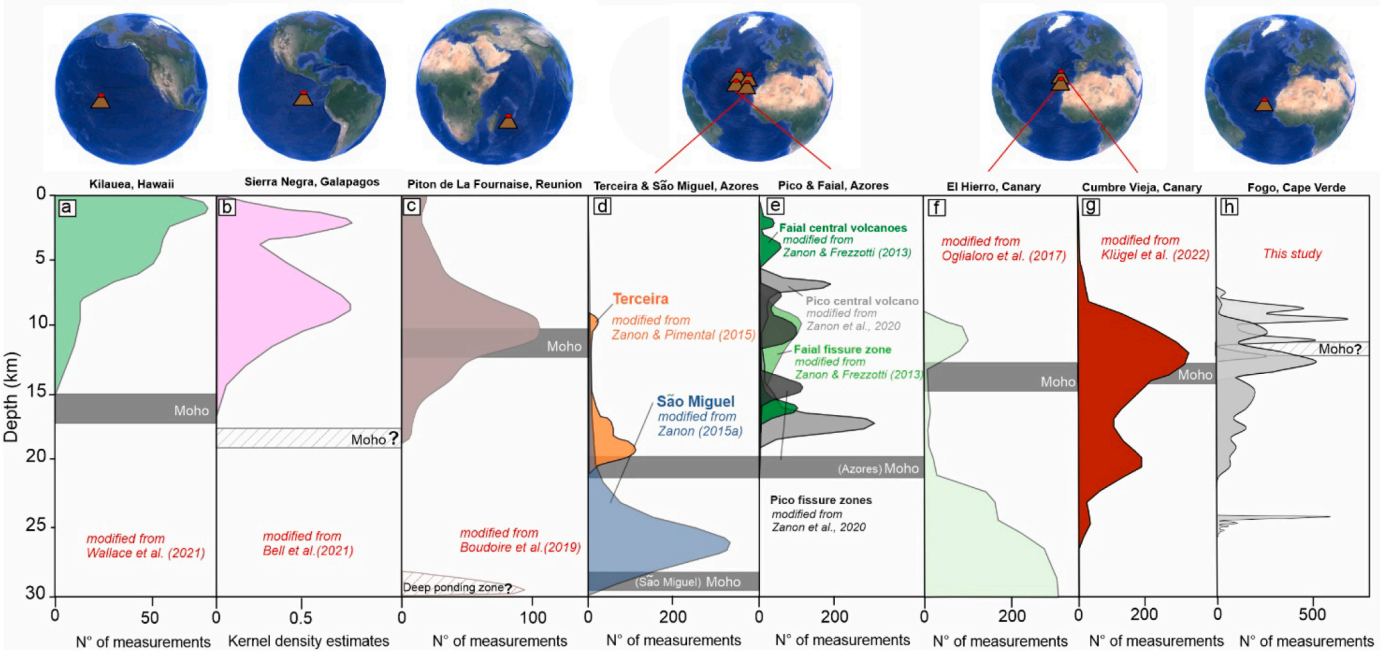

Fig. 7. Plumbing systems barometric studies for contrasting types of mafic volcanoes (Analytics method: melt inclusions entrapment pressure, a; olivine-augite-plagioclase-melt (OPAM) barometer, b; fluid inclusions Raman densimeter and clinopyroxene-melt barometer, c; fluid inclusions microthermometry, d,e,f,g,h). The two volcanoes Kilauea (a) and Sierra Negra (b), in the Pacific Ocean, and Piton de La Fournaise (c) in the Indian Ocean, record barometric ranges that show a shallow storage zone <6 km depth. Contrary, Terceira, São Miguel, Pico and Faial (d,e) (Azores Archipelago), El Hierro (f) and La Palma (g) (Canary Islands), and Fogo (h) (Cape Verde), have in common the presence of a deepest magma zone at- 15–30 km depth.

erupted magmas were initially sourced in reservoirs at 17–25 km, our results concur to suggest pre-eruptive prolonged stalling of magmas starting from 17 km. Such longer residence times in the oceanic crust would be consistent with the slightly evolved nature ($SiO_2 > 42$ wt%; $FeO/MgO > 2.0$) of the erupted lavas relative to 1600s–1800s volcanics.

Pico do Fogo has been frequently active since the 1400s and it is therefore possible that such repeated pulses of magma ascent through the central feeding system have locally altered the thermal properties of the ocean crust, causing magma stalling at progressively shallower depths over time. Magma mixing during prolonged shallow magma residence would also fit with clinopyroxene textural features (e.g., rounded, or embayed cores overgrown by euhedral and zoned clinopyroxene, that show disequilibrium) and with the recurrent eruption of gabbroic xenoliths by lavas (Hildner et al., 2012).

Our data suggests the magmatic system is evolving towards a state in which magma is drained from the uppermost portion of the 17–25 km source area, but then stalls at ~9–17 km depth shortly before eruption. In any future unrest, this process should be traceable as a progressive escalation of increasingly shallow seismicity, as seen elsewhere (e.g., D'Auria et al., 2022).

5.4. Comparison with the magma system at other ocean island volcanoes

In the last two decades, fluid inclusions microthermometry has been used to define the architecture of many oceanic volcanoes. In Fig. 7 the magma system at Fogo is compared with the data from Kilauea (Hawaii) and Sierra Negra (Galápagos) in the Pacific Ocean, Piton de La Fournaise (Réunion Island) in the Indian Ocean, and El Hierro and La Palma (Canary Islands), Pico, Faial, Terceira, and São Miguel (Azores Islands) in the Atlantic Ocean. For each volcanic system, we use literature data derived from fluid inclusions microthermometry, but also petrological/geophysical information where fluid inclusion results are unavailable.

Fig. 7 demonstrates magma storage conditions ranging from shallow crustal (e.g., Kilauea) to upper mantle (e.g., El Hierro). This diversity is not unexpected if it considered the large range of key parameters that govern magma ascent and storage at the volcanoes used for the comparison, such as:

(i) crust thickness ranging from ~27 to 29 km underneath São Miguel (Zanon, 2015a), to ~12–15 km underneath Canary volcanoes (D'Auria et al., 2022; Ranero et al., 1995) and crust age ranging from ~155 Ma below La Palma (Verhoef et al., 1991) to <5 Ma beneath the Galápagos (White et al., 1993);
(ii) magma supply rate ranging from 3 to 4 $m^3 \cdot s^{-1}$ at Kilauea (Poland, 2014), to 0.06 $m^3 \cdot s^{-1}$ at Fogo (Bagnardi et al., 2016);
(iii) magma geochemistry varying from subalkaline/mildly alkaline basalts at the Azores (Zanon, 2015b) to basanites at Cape Verde and at the Canary (Mata et al., 2017; Klügel et al., 2022; Stroncik et al., 2009);
(iv) central volcano vs fissure zone. The first kind is due to the intersection of local tectonic systems and is a frequent cause for the formation of ephemeral shallow and small magma accumulation zones. The second kind is associated with extensional or trans-extensional tectonics and favours the direct tapping of deep magma accumulation zones and magma rapid ascent. These two kinds frequently coexist in the same island, generating overlapping data (e.g., Piton de La Fournaise, the Azores, Kilauea).

As a result, it is possible to envisage three categories of volcanos at oceanic setting:

a first group includes the plume fed volcanoes of Kilauea and Sierra Negra where data evidence only a shallow magma storage zone in the upper crust (Fig. 7a,b). At Kilauea, melt inclusion results point to shallow magma storage conditions, ranging from 1 to 5 km depth (Lerner et al., 2021) to 2–3 km depth (Wieser et al., 2021). Volcanic rock geochemistry, seismic and geodetic evidence (Bell et al., 2021), and volcanic gas compositions (Aiuppa et al., 2022), likewise show shallow magma ponding at ~2 km depth below Sierra Negra caldera (Galápagos Archipelago) during volcano repose. At these volcanoes, the high supply rate, e.g., 3–4 $m^3 \cdot s^{-1}$ as is the case of Kilauea (Poland, 2014), allow primitive magmas to ascend with ease through the "hot" crustal section, to only stall in a shallow magma storage zone (Lerner et al., 2020; Wallace et al., 2021).

A second group includes the fissure zone systems of the volcanoes of the Azores and of La Reunion Island. These systems are dominated by extensional to trans-extensional tectonics. Poorly evolved to primitive magmas directly ascend from the deepest accumulation zones, which are located at the Moho (Fig. 7c,d,e). Where these fissure systems are intersected by local tectonics, the direct magma ascent is hampered and small intra-crustal magma accumulation zones form (Boudoire et al., 2019; Zanon, 2015b). At Piton de La Fournaise, magma supply is high, and the shallow system is replenished and tapped by frequent eruptions, so that the evolution degree is very limited. At the Azores, intruded volumes are scarce and magma evolution is extreme and the intra-crustal accumulation zone consists of small lenses of syenites.

The last group includes El Hierro and La Palma (Cumbre Vieja) fissure systems. At these volcanic systems FIAs entrapment conditions reveal a deep magma accumulation zone at a depth from 25 to 30 km (Oglialoro et al., 2017; Klügel et al., 2022) where basanites stall (Fig. 7f, g). A main intra-crustal storage area (10–15 km) which is present at the scale of the whole islands, is the responsible for the magmatic evolution towards tephrites to phonolites, as a function of magma supply rate.

Ultimately, this comparison shows that the magma system below Fogo Volcano resemble that of Cumbre Vieja (Fig. 7h). We propose that a combination of low magma supply rates (0.06 $m^3 \cdot s^{-1}$, Bagnardi et al., 2016) and a "cold" nature of the ~125 Ma-old oceanic crust beneath the volcano (Courtney and White, 1986), concur to cause cooling, crystallization and stalling of magmas in the deep crust, and/or at the crust/mantle interface (Hildner et al., 2012), and prevent from shallow magma reservoirs to form. This lack is consistent with geophysical data recorded before and during more recent eruptions, including: (i) the absence of volcano-wide deformation (inflation/deflation cycles) prior, during and after the 1995 and 2014–15 eruptions (Amelung and Day, 2002; González et al., 2015), and (ii) the deep nature (hypocentres at ~17 km b.s.l.) of precursor seismicity observed before the 2014–15 eruption (Mata et al., 2017). However, FIAs in gabbroic xenoliths from the 1951 eruption show a crystallization zone at ~2–7 km depth, which is probably limited only to the eruptive site.

5.5. Caveats and limitations

Our results have provided some advance in the understanding of magma feeding processes at Fogo - yet we acknowledge several limitations still exist that prevent us from obtaining a comprehensive and unitary view of the plumbing system.

The representativity of data is a main concern. Despite ~2700 fluid inclusions were analysed from 11 eruptions, only 1–3 crystals per eruption were studied. Therefore, the extent to which the few mineral grains analysed represent of the fluid entrapment conditions of the entire population of crystals (all/most containing FIAs) of an eruption remains uncertain. We have characterised some of the historical eruptions, but many others remain unstudied. Further studies are needed before the structure and temporal evolution of the magma system can be fully understood.

Another source of uncertainty is the assumption that the inclusions contain 10 mol% H_2O (cfr. 3). If deep fluids did not contain 10 mol% H_2O, the pressure/depth estimates would be lower. However, the Fogo basanites are hydrous (up to >2.5 wt% H_2O measured in deeply trapped melt inclusions; Moussallam et al., 2019) relative to other volcanoes (e.g., Kilauea; Lerner et al., 2020; Wallace et al., 2021). At such conditions, degassing model calculations, performed by initialising the Moretti et al. (2003) saturation code with parental melt compositions appropriate for

Fogo (e.g., using the melt inclusion results of Moussallam et al., 2019), show that the magmatic fluid phase in equilibrium with the melt in the 250–400 MPa pressure range contains from ~5 to ~10 mol% H_2O, overall justifying the correction method adopted.

Finally, Type II FIAs are here interpreted as the result re-equilibration of Type I inclusions upon ascent, in which the fluid delivered by Type I inclusions is re-entrapped as trails of lower density bubbles along crystal fractures. We caution that such re-equilibration, and density resetting to the new (lower) external pressures, may only be partial and not complete, in which case our inferred pressures for Type II FIAs would in fact over-estimate the real depths at which re-equilibration takes place.

6. Conclusions

The evolution of magma system underneath Fogo Volcano has been previously characterised by fluid inclusions microthermometry and clinopyroxene–melt-barometry, only for a limited dataset of recent eruptions. The barometric results presented here extend this analysis to ~120 ka and contribute to reconstruct the temporal history of the Fogo magma system, which, according to the resulting conceptual model (Fig. 8), evolved over the last 120 ka.

The ~120 ka eruption, pre-dating the Monte Amarelo collapse event, emitted basanite magma stored at a depth of ~19–22 km. Results for the ~60 ka early post-collapse eruption bring evidence for the direct magma withdrawal from the deepest storage system at ~24 km, suggesting that after the collapse, magma extraction bypassed the shallower magma system. FIAs in Holocene/historical eruptions show, instead, slower magma ascent rates, and more prolonged magma storage in the 13–17 km depth range (as shown by Type I fluid inclusions). Shallow re-equilibration of FIAs takes place at 9–12 km depth, as shown by Type II FIAs.

The picture that emerges from our study reinforces earlier conclusions for the recent (< 10 ka) activity being modulated by dynamics of magma stored at ~13–25 km. The geometry of this ~13–25 km magma storage zone is unconstrained, but the diverse entrapment and re-equilibration events identified for the various historical Fogo eruptions, and the small volumes erupted, concur to suggest the existence of small-volume magma pockets interspersed within a well-established crystal mush zone, overall giving rise to a vertically extended trans-crustal magmatic system (Fig. 8c). Our results suggest the magma storage conditions and ascent pathways at Fogo are eruption-specific, which means that the plumbing system is made of several small, interconnected magma lenses, rather than by a single melt-dominated reservoir. We thus provide additional support to modern views of magma systems that argue in favour of the existence of multiple, superimposed ponding levels in which magma is only temporarily stored during its journey towards the surface.

The magma system of Fogo would, therefore, share features with many oceanic volcanoes in which a series of small magma lenses at deep crustal to upper mantle depths feed transient crustal magma ponding zones during rapid (days/weeks) pre-eruptive emplacement. In contrast

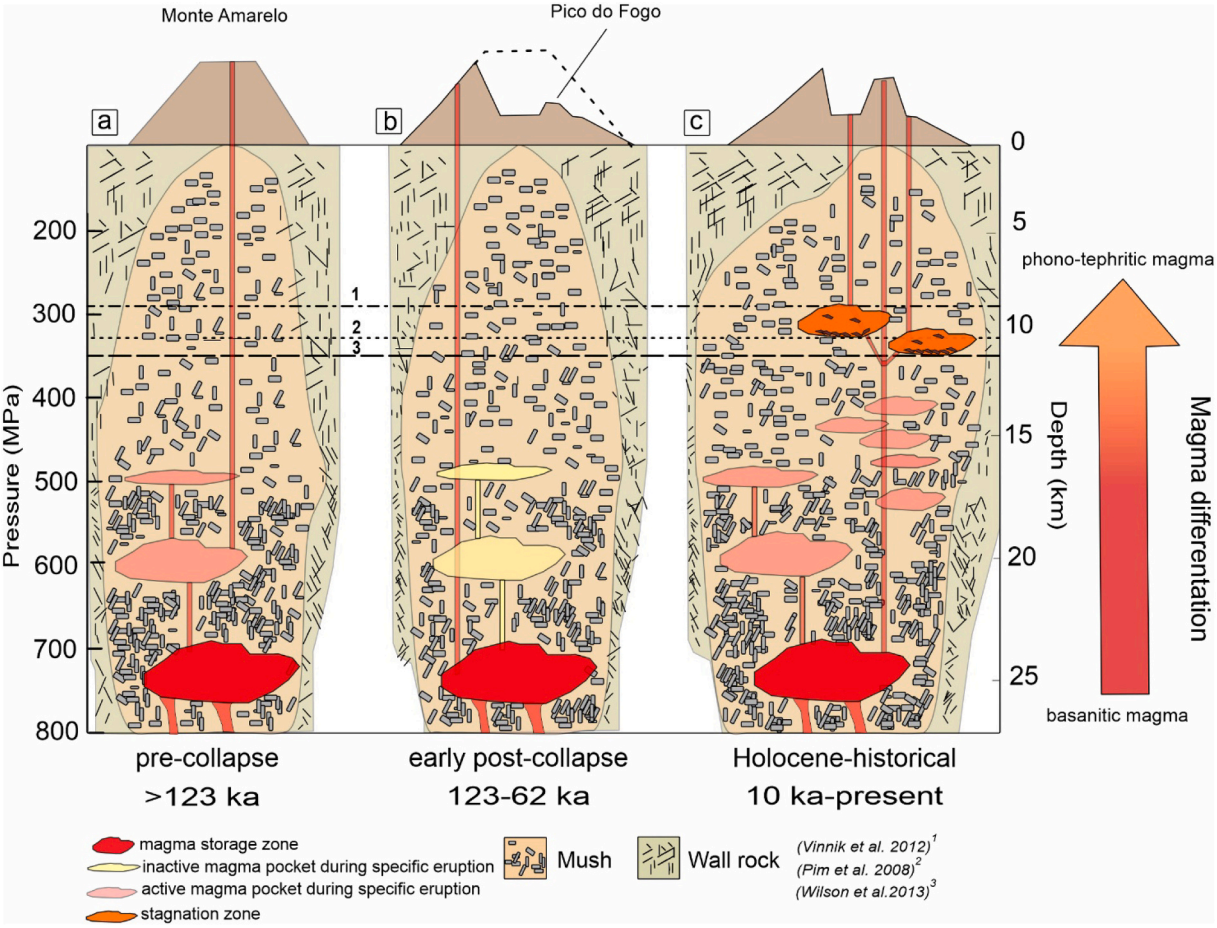

Fig. 8. Schematic cross-sections of Fogo Island (not to scale), showing the temporal evolution of the magma feeding system during (a) pre-collapse, (b) early post-collapse and (c) Holocene/historical activity. FIAs in Holocene-historical eruptions suggest longer residence in a shallower magma ponding zone prior to eruption, at the inferred fossil Moho (1) and/or at the upper mantle-crust transition (2,3). More evolved melts (e.g., phono-tephrites) may form in this region by fractional crystallization. The ~19 km and ~ 15–17 km regions are interpreted as parts of a vertically extended magma system, in which several interconnected ponding zones exist that are periodically refilled during specific eruptions. The main region of magma storage is at ~23.7 ± 0.9 km.

to some ocean island volcanoes with persistent shallow magma storage regions (e.g., Kilauea, Sierra Negra), the lack of Type I inclusions at depths <13 km points against any long-lived magma storage at shallow crustal levels. However, the apparent upward migration of magma storage conditions observed since the 1951 eruption (Fig. 8), if corroborated by additional results, may suggest a tendency towards a more mature, central-volcano activity phase, in which shallow crustal processing of magma is becoming more important with time. The fluid inclusion results provide a guide to the deep depths of magma storage at Fogo and the short transit time to the surface. This information aids the interpretation of earthquake locations and other monitoring information. Our study thus provides crucial information for future assessment of volcanic risk and hazard mitigation at Fogo, where the two last eruptions have proven catastrophic for local communities.

CRediT authorship contribution statement

Francesco Maria Lo Forte: Data curation, Investigation, Software, Writing – original draft, Visualization, Writing – review & editing. **Alessandro Aiuppa:** Funding acquisition, Writing – original draft, Writing – review & editing. **Silvio G. Rotolo:** Investigation, Writing – review & editing. **Vittorio Zanon:** Funding acquisition, Conceptualization, Methodology, Supervision, Validation, Writing – original draft, Writing – review & editing.

Declaration of Competing Interest

The authors declare the following financial interests/personal relationships which may be considered as potential competing interests:

Alessandro Aiuppa reports financial support was provided by MIUR. Vittorio Zanon reports financial support was provided by Fundação para a Ciência e Tecnologia. Alessandro Aiuppa reports financial support was provided by Alfred P Sloan Foundation.

Data availability

Data will be made available on request.

Acknowledgements

This research received financial support from the Deep Carbon Observatory (Alfred P. Sloan Foundation, USA), the Ministero dell'Università e Ricerca (Italy, Grant n. 2017LMNLAW) and the research project MAGAT - From MAGma to the ATmosphere - a contribution to develop the next generation of geochemical sensors for real-time monitoring of magma movement at depth (CIRCNA/OCT/0016/2019), funded by the Fundação para a Ciência e Tecnologia, Portugal. The Instituto de Investigação em Vulcanologia e avaliação de riscos (IVAR) is ackowledged for hosting FLF. Alan Lerner and an anonymous reviewer provided useful comments that significantly improved the quality of the manuscript. The editor Tobias Fischer is acknowledged for the handling of this paper.

Appendix A. Supplementary data

Supplementary data to this article can be found online at https://doi.org/10.1016/j.jvolgeores.2022.107730.

References

Aiuppa, A., Allard, P., Bernard, B., Lo Forte, F.M., Moretti, R., Hidalgo, S., 2022. Gas leakage from shallow ponding magma and trapdoor faulting at Sierra Negra volcano (Isabela Island, Galápagos). Geochem. Geophys. Geosyst. 23, e2021GC010288 https://doi.org/10.1029/2021GC010288.

Amelung, F., Day, S., 2002. InSAR observations of the 1995 Fogo, Cape Verde, eruption: Implications for the effects of collapse events upon island volcanoes. Geophys. Res. Lett. 29, 1606. https://doi.org/10.1029/2001GL013760.

Bagnardi, M., González, P.J., Hooper, A., 2016. High-resolution digital elevation model from tri-stereo Pleiades-1 satellite imagery for lava flow volume estimates at Fogo Volcano. Geophys. Res. Lett. 43 (12), 6267–6275.

Bakker, R.J., 2003. Package FLUIDS 1. Computer programs for analysis of fluid inclusion data and for modelling bulk fluid properties. Chem. Geol. 194, 3–23. https://doi.org/10.1016/S0009-2541(02)00268-1.

Barth, A., Newcombe, M., Plank, T., Gonnermann, H., Hajimirza, S., Soto, G.J., Saballos, A., Hauri, E., 2019. Magma decompression rate correlates with explosivity at basaltic volcanoes — Constraints from water diffusion in olivine. J. Volcanol. Geotherm. Res. 387, 106664 https://doi.org/10.1016/j.jvolgeores.2019.106664.

Bell, A.F., La Femina, P.C., Ruiz, M., Amelung, F., Bagnardi, M., Bean, C.J., Bernard, B., Ebinger, C., Gleeson, M., Grannell, J., Hernandez, S., Higgins, M., Liorzou, C., Lundgren, P., Meier, N.J., Möllhoff, M., Oliva, S.-J., Ruiz, A.G., Stock, M.J., 2021. Caldera resurgence during the 2018 eruption of Sierra Negra volcano, Galápagos Islands. Nat. Commun. 12, 1397. https://doi.org/10.1038/s41467-021-21596-4.

Biggs, J., Ebmeier, S.K., Aspinall, W.P., Lu, Z., Pritchard, M.E., Sparks, R.S.J., Mather, T. A., 2014. Global link between deformation and volcanic eruption quantified by satellite imagery. Nat. Commun. 5, 3471. https://doi.org/10.1038/ncomms4471.

Bodnar, R.J., 2003. Introduction to fluid inclusions. In: Samson, I., Anderson, A., Marshall, D. (Eds.), Fluid Inclusions: Analysis and Interpretation. Assoc. Canada, Short Course 32, pp. 1–8.

Boudoire, G., Brugier, Y.-A., Di Muro, A., Wörner, G., Arienzo, I., Metrich, N., Zanon, V., Braukmüller, N., Kronz, A., Le Moigne, Y., Michon, L., 2019. Eruptive activity on the Western Flank of Piton de la Fournaise (La Réunion Island, Indian Ocean): insights on magma transfer, storage and evolution at an Oceanic Volcanic Island. J. Petrol. 60, 1717–1752. https://doi.org/10.1093/petrology/egz045.

Caricchi, L., Sheldrake, T.E., Blundy, J., 2018. Modulation of magmatic processes by CO2 flushing. Earth Planet. Sci. Lett. 491, 160–171.

Carlson, R.L., Raskin, G.S., 1984. Density of the ocean crust. Nature 311, 555–558. https://doi.org/10.1038/311555a0.

Carracedo, J.C., 1999. Growth, structure, instability and collapse of Canarian volcanoes and comparisons with Hawaiian volcanoes. J. Volcanol. Geotherm. Res. 94 (1–4), 1–19.

Carracedo, J.-C., Perez-Torrado, F.J., Rodriguez-Gonzalez, A., Paris, R., Troll, V.R., Barker, A.K., 2015. Volcanic and structural evolution of Pico do Fogo, Cape Verde. Geol. Today 31, 146–152. https://doi.org/10.1111/gto.12101.

Cashman, K.V., Edmonds, M., 2019. Mafic glass compositions: a record of magma storage conditions, mixing and ascent. Philos. Trans. R. Soc. A Math. Phys. Eng. Sci. 377, 20180004. https://doi.org/10.1098/rsta.2018.0004.

Cashman, K.V., Giordano, G., 2014. Calderas and magma reservoirs. J. Volcanol. Geotherm. Res. 288, 28–45. https://doi.org/10.1016/j.jvolgeores.2014.09.007.

Cashman, K.V., Sparks, R.S.J., Blundy, J.D., 2017. Vertically extensive and unstable magmatic systems: a unified view of igneous processes. Science 355, eaag3055. https://doi.org/10.1126/science.aag3055.

Cooper, K.M., Kent, A.J.R., 2014. Rapid remobilization of magmatic crystals kept in cold storage. Nature 506, 480–483. https://doi.org/10.1038/nature12991.

Cooper, A.K., Marlow, M.S., Scholl, D.W., Stevenson, A.J., 1992. Evidence for cenozoic crustal extension in the Bering Sea region. Tectonics 11, 719–731. https://doi.org/10.1029/92TC00214.

Courtney, R.C., White, R.S., 1986. Anomalous heat flow and geoid across the Cape Verde rise: evidence for dynamic support from a thermal plume in the mantle. Geophys. J. Int. 87, 815–867. https://doi.org/10.1111/j.1365-246X.1986.tb01973.x.

Dash, B.P., Ball, M.M., King, G.A., Butler, L.W., Rona, P.A., 1976. Geophysical investigation of the Cape Verde Archipelago. J. Geophys. Res. 81, 5249–5259. https://doi.org/10.1029/JB081i029p05249.

D'Auria, L., Koulakov, I., Prudencio, J., Cabrera-Perez, I., Ibáñez, J., Barrancos, J., Hernandez, R.G., Van Dorth, D.M., Hernandez, G.P., Przeor, M., Ortega, V., Perez, P. H., Rodriguez, N.P., 2022. Voluminous storage and Rapid magma ascent beneath La Palma revealed by seismic Tomography. Res. Square. https://doi.org/10.21203/rs.3.rs-1238072/v1.

Day, S.J., Heleno da Silva, S.I.N., Fonseca, J.F.B.D., 1999. A past giant lateral collapse and present-day flank instability of Fogo, Cape Verde Islands. J. Volcanol. Geotherm. Res. 94, 191–218. https://doi.org/10.1016/S0377-0273(99)00103-1.

Day, S.J., Carracedo, J.C., Guillou, H., Pais Pais, F.J., Badiola, E.R., Fonseca, J.F.B.D., Heleno, S.I.N., 2000. Comparison and cross-checking of historical, archaeological and geological evidence for the dilocation and type of historical and sub-historical eruptions of multiple-vent oceanic island volcanoes. Geol. Soc. Lond. Spec. Publ. 171, 281–306. https://doi.org/10.1144/GSL.SP.2000.171.01.21.

Dixon, J.E., Stolper, E.M., 1995. An experimental study of water and carbon dioxide solubilities in mid-ocean ridge basaltic liquids. Part II: applications to degassing. J. Petrol. https://doi.org/10.1093/oxfordjournals.petrology.a037268.

Edmonds, M., Cashman, K.V., Holness, M., Jackson, M., 2019. Architecture and dynamics of magma reservoirs. Philos. Trans. R. Soc. A Math. Phys. Eng. Sci. 377, 20180298. https://doi.org/10.1098/rsta.2018.0298.

Foeken, J., Stuart, F., Day, S., Wall, F., 2007. Carbonatite seamount formation and first subaerial exposure of Fogo (Cape Verde Islands): results from apatite and pyrochlore (U–Th)/He dating. Geophys. Res. Abstr. 9. EGU2007-A-09688.

Foeken, J.P.T., Day, S., Stuart, F.M., 2009. Cosmogenic 3He exposure dating of the Quaternary basalts from Fogo, Cape Verdes: implications for rift zone and magmatic reorganisation. Quat. Geochronol. 4, 37–49. https://doi.org/10.1016/j.quageo.2008.07.002.

Foroozan, R., Elsworth, D., Voight, B., Mattioli, G.S., 2010. Dual reservoir structure at Soufrière Hills Volcano inferred from continuous GPS observations and heterogeneous elastic modeling. Geophys. Res. Lett. 37 https://doi.org/10.1029/2010GL042511.

Frezzotti, M.L., Peccerillo, A., 2004. Fluid inclusion and petrological studies elucidate reconstruction of magma conduits. Transactions of the American Geophysical Union 85 (16), 157–163. https://doi.org/10.1029/2004EO160001.
Frezzotti, M.L., Tecce, F., Casagli, A., 2012. Raman spectroscopy for fluid inclusion analysis. J. Geochem. Explor. 112, 1–20. https://doi.org/10.1016/j.gexplo.2011.09.009.
Galipp, K., Klügel, A., Hansteen, T.H., 2006. Changing depths of magma fractionation and stagnation during the evolution of an oceanic island volcano: La Palma (Canary Islands). J. Geophys. Res. 155, 285–306. https://doi.org/10.1016/j.jvolgeores.2006.04.002.
Gerlach, D.C., Cliff, R.A., Davies, G.R., Norry, M., Hodgson, N., 1988. Magma sources of the Cape Verdes archipelago: Isotopic and trace element constraints. Geochim. Cosmochim. Acta 52, 2979–2992. https://doi.org/10.1016/0016-7037(88)90162-7.
Goldstein, R.H., Samson, I., Anderson, A., Marshall, D., 2003. Petrographic analysis of fluid inclusions. In: Fluid Inclusions: Analysis and Interpretation, 32, pp. 9–53.
González, P.J., Bagnardi, M., Hooper, A.J., Larsen, Y, Marinkovic, P., Samsonov, S.V., Wright, T.J., 2015. The 2014–2015 eruption of Fogo volcano: Geodetic modeling of Sentinel-1 TOPS interferometry. Geophys. Res. Lett. 42, 9239–9246. https://doi.org/10.1002/2015GL066003.
Hansteen, T.H., Klugel, A., 2008. Fluid inclusion thermobarometry as a tracer for magmatic processes. Rev. Mineral. Geochem. 69, 143–177. https://doi.org/10.2138/rmg.2008.69.5.
Hansteen, T.H., Klügel, A., Schmincke, H.-U., 1998. Multi-stage magma ascent beneath the Canary Islands: evidence from fluid inclusions. Contrib. Mineral. Petrol. 132, 48–64. https://doi.org/10.1007/s004100050404.
Hildner, E., Klügel, A., Hauff, F., 2011. Magma storage and ascent during the 1995 eruption of Fogo, Cape Verde Archipelago. Contrib. Mineral. Petrol. 162, 751–772. https://doi.org/10.1007/s00410-011-0623-6.
Hildner, E., Klügel, A., Hansteen, T.H., 2012. Barometry of lavas from the 1951 eruption of Fogo, Cape Verde Islands: Implications for historic and prehistoric magma plumbing systems. J. Volcanol. Geotherm. Res. 217–218, 73–90. https://doi.org/10.1016/j.jvolgeores.2011.12.014.
Hoernle, K., Tilton, G., Le Bas, M.J., Duggen, S., Garbe-Schönberg, D., 2002. Geochemistry of oceanic carbonatites compared with continental carbonatites: mantle recycling of oceanic crustal carbonate. Contrib. Mineral. Petrol. 142, 520–542. https://doi.org/10.1007/s004100100308.
Holtzman, B.K., Kohlstedt, D.L., 2007. Stress-driven melt segregation and strain partitioning in partially molten rocks: effects of stress and strain. J. Petrol. 48, 2379–2406. https://doi.org/10.1093/petrology/egm065.
Klügel, A., Hansteen, T.H., Galipp, K., 2005. Magma storage and underplating beneath Cumbre Vieja volcano, La Palma (Canary Islands). Earth Planet. Sci. Lett. 236, 211–226. https://doi.org/10.1016/j.epsl.2005.04.006.
Klügel, A., Day, S., Schmid, M., Faria, B., 2020. Magma plumbing during the 2014–2015 eruption of Fogo (Cape Verde Islands). Front. Earth Sci. 8, 157. https://doi.org/10.3389/feart.2020.00157.
Klügel, A., Albers, E., Hansteen, T.H., 2022. Mantle and Crustal Xenoliths in a Tephriphonolite from La Palma (Canary Islands): implications for phonolite formation at Oceanic Island Volcanoes. Front. Earth Sci. 10, 761902 https://doi.org/10.3389/feart.2022.761902.
Lénat, J.-F., Bachelery, P., 1990. Structure et fonctionnement de la zone centrale du Piton de la Fournaise. In: Le volcanisme de la Reunion, Monographie. Cent. Rech. Volc, Clermont-Ferrand, pp. 257–296.
Lerner, A.H., O'Hara, D., Karlstrom, L., Ebmeier, S.K., Anderson, K.R., Hurwitz, S., 2020. The prevalence and significance of offset magma reservoirs at arc volcanoes. Geophys. Res. Lett. 47, e2020GL087856.
Lerner, A.H., Wallace, P., Shea, T., 2021. The petrologic and degassing behavior of sulfur and other magmatic volatiles from the 2018 erup-tion of Kīlauea, Hawai'i: Melt concentrations, magma storage depths, and magma recycling. Bull. Volcanol. 83 (43), 1–32. https://doi.org/10.1007/s00445-021-01459-y.
Liu, X., Zhao, D., 2014. Seismic evidence for a mantle plume beneath the Cape Verde hotspot. Int. Geol. Rev. 56, 1213–1225. https://doi.org/10.1080/00206814.2014.930720.
Magnusson, E., 2016. Temporal Evolution of Historic Mafic Lavas from Fogo, Cape Verde. MSc Thesis. Uppsala University, Uppsala, Sweden.
Manconi, A., Longpre, M.-A., Walter, T.R., Troll, V.R., Hansteen, T.H., 2009. The effects of flank collapses on volcano plumbing systems. Geology 37, 1099–1102. https://doi.org/10.1130/G30104A.1.
Martínez-Moreno, F.J., Monteiro Santos, F.A., Madeira, J., Pous, J., Bernardo, I., Soares, A., Esteves, M., Adão, F., Ribeiro, J., Mata, J., Brum da Silveira, A., 2018. Investigating collapse structures in oceanic islands using magnetotelluric surveys: the case of Fogo Island in Cape Verde. J. Volcanol. Geotherm. Res. 357, 152–162. https://doi.org/10.1016/j.jvolgeores.2018.04.028.
Mata, J., Martins, S., Mattielli, N., Madeira, J., Faria, B., Ramalho, R.S., Silva, P., Moreira, M., Caldeira, R., Moreira, M., Rodrigues, J., Martins, L., 2017. The 2014–15 eruption and the short-term geochemical evolution of the Fogo volcano (Cape Verde): evidence for small-scale mantle heterogeneity. Lithos 288–289, 91–107. https://doi.org/10.1016/j.lithos.2017.07.001.
Mattioli, G.S., Herd, R.A., Strutt, M.H., Ryan, G., Widiwijayanti, C., Voight, B., 2010. Long term surface deformation of Soufrière Hills Volcano, Montserrat from GPS geodesy: Inferences from simple elastic inverse models. Geophys. Res. Lett. 37 https://doi.org/10.1029/2009GL042268.
Menand, T., 2011. Physical controls and depth of emplacement of igneous bodies: a review. Tectonophysics 500 (1–4), 11–19. https://doi.org/10.1016/j.tecto.2009.10.016.
Métrich, N, Wallace, P.J., 2008. Volatile Abundances in Basaltic Magmas and Their Degassing Paths Tracked by Melt Inclusions. Rev. Mineral. Geochem. 69, 363–402. https://doi.org/10.2138/RMG.2008.69.10.
Moretti, R., Papale, P., Ottonello, G., 2003. In: Oppenheimer, C., Pyle, D.M., Barclay, J. (Eds.), A Model for the Saturation of C-H-O-S Fluids in Silicate Melts, vol. 213. Geological Society of London Special Publication. Volcanic Degassing, pp. 81–101. https://doi.org/10.1144/GSL.SP.2003.213.01.06.
Mourão, C., Moreira, M., Mata, J., Raquin, A., Madeira, J., 2012. Primary and secondary processes constraining the noble gas isotopic signatures of carbonatites and silicate rocks from Brava Island: evidence for a lower mantle origin of the Cape Verde plume. Contrib. Mineral. Petrol. 163, 995–1009. https://doi.org/10.1007/s00410-011-0711-7.
Moussallam, Y., Longpré, M.-A., McCammon, V., Gomez-Ulla, A., Rose-Koga, E.F., Scaillet, B., Peters, N., Gennaro, E., Paris, R., Oppenheimer, C:, 2019. Mantle plumes are oxidised. Earth Planet. Sci. Lett. 527, 115798. https://doi.org/10.1016/j.epsl.2019.115798.
Neave, D.A., Beckmann, P., Behrens, H., Holtz, F., 2021. Mixing between chemically variable primitive basalts creates and modifies crystal cargoes. Nat. Commun. 12, 5495. https://doi.org/10.1038/s41467-021-25820-z.
Oglialoro, E., Frezzotti, M., Ferrando, S., Tiraboschi, C., Principe, C., Groppeli, G., Villa, I.M., 2017. Lithospheric magma dynamics beneath the El Hierro Volcano, Canary Islands: insights from fluid inclusions. Bull. Volcanol. 79, 70. https://doi.org/10.1007/s00445-017-1152-6.
Pappalardo, L., Buono, G., 2021. Insights into processes and timescales of magma storage and ascent from textural and geochemical investigations: Case studies from high-risk Neapolitan Volcanoes (Italy). In: Masotta, M., Beier, C., Mollo, S. (Eds.), Geophysical Monograph Series. Wiley, pp. 213–235. https://doi.org/10.1002/9781119564485.ch10.
Parmigiani, A., Huber, C., Bachmann, O., 2014. Mush microphysics and the reactivation of crystal-rich magma reservoirs. J. Geophys. Res. Solid Earth 119, 6308–6322. https://doi.org/10.1002/2014JB011124.
Pim, J., Peirce, C., Watts, A.B., Grevemeyer, I., Krabbenhoeft, A., 2008. Crustal structure and origin of the Cape Verde rise. Earth Planet. Sci. Lett. 272, 422–428. https://doi.org/10.1016/j.epsl.2008.05.012.
Poland, M.P., 2014. Time-averaged discharge rate of subaerial lava at Kīlauea Volcano, Hawai'i, measured from TanDEM-X interferometry: Implications for magma supply and storage during 2011–2013. J. Geophys. Res. Solid Earth 119, 5464–5481. https://doi.org/10.1002/2014JB011132.
Putirka, K.D., 2008. Thermometers and Barometers for Volcanic Systems. Rev. Mineral. Geochem. 69, 61–120. https://doi.org/10.2138/rmg.2008.69.3.
Putirka, K.D., Perfit, M., Ryerson, F.J., Jackson, M.G., 2007. Ambient and excess mantle temperatures, olivine thermometry, and active vs. passive upwelling. Chem. Geol. 241, 177–206. https://doi.org/10.1016/j.chemgeo.2007.01.014.
Ranero, C.R., Torne, M., Banda, E., 1995. Gravity and multichannel seismic reflection constraints on the lithospheric structure of the Canary Swell. Mar. Geophys. Res. 17, 519–534. https://doi.org/10.1007/BF01204342.
Rhodes, J.M., Dungan, M.A., Blanchard, D.P., Long, P.E., 1979. Magma mixing at mid-ocean ridges: evidence from basalts drilled near 22° N on the Mid-Atlantic Ridge. Tectonophysics 55, 35–61. https://doi.org/10.1016/0040-1951(79)90334-2.
Ribeiro, O., 1954. A Ilha Do Fogo e as suas erupções. Junta de Investigações do Ultramar, Lisbon.
Roedder, E., 1984. Fluid inclusions. Reviews in Mineralogy, 12. Mineralogical Society of America, pp. 1–644.
Schwarz, S., Klügel, A., Wohlgemuth-Ueberwasser, C., 2004. Melt extraction pathways and stagnation depths beneath the Madeira and Desertas rift zones (NE Atlantic) inferred from barometric studies. Contrib. Mineral. Petrol. 147, 228–240. https://doi.org/10.1007/s00410-004-0556-4.
Siebert, L., Simkin, T., 2002. Volcanoes of the World: An Illustrated Catalog of Holocene Volcanoes and their Eruptions. In: Global Volcanism Program Digital Information Series. Smithsonian Institution.
Span, R., Wagner, W., 1996. A new equation of state for carbon dioxide covering the fluid region from the triple-point temperature to 1100 K at pressures up to 800 MPa. J. Phys. Chem. Ref. Data 25, 1509–1596. https://doi.org/10.1063/1.555991.
Sparks, R.S.J., Annen, C., Blundy, J.D., Cashman, K.V., Rust, A.C., Jackson, M.D., 2019. Formation and dynamics of magma reservoirs. Philos. Trans. R. Soc. A Math. Phys. Eng. Sci. 377, 20180019. https://doi.org/10.1098/rsta.2018.0019.
Sterner, S.M., Bodnar, R.J., 1991. Synthetic fluid inclusions; X, experimental determination of P-V-T-X properties in the CO2-H2O system to 6 kb and 700 degrees C. Am. J. Sci. 291, 1–54. https://doi.org/10.2475/ajs.291.1.1.
Stroncik, N.A., Klügel, A., Hansteen, T.H., 2009. The magmatic plumbing system beneath El Hierro (Canary Islands): constraints from phenocrysts and naturally quenched basaltic glasses in submarine rocks. Contrib. Mineral. Petrol. 157, 593–607. https://doi.org/10.1007/s00410-008-0354-5.
Tenzer, R., Bagherbandi, M., Vajda, P., 2013. Global model of the upper mantle lateral density structure based on combining seismic and isostatic models. Geosci. J. 17, 65–73. https://doi.org/10.1007/s12303-013-0009-z.
Torres, P., Madeira, J., Silva, L., Brum da Silveira, A., Serraheíro, A., Mota Gomes, A., 1997. Carta Geológica das Erupções Históricas da Ilha do Fogo (Cabo Verde): revisão e actualização Comn. Inst. Geol. Mine. 84, A193–A196.
Torres, P., Silva, L.C., Munhá, J., Caldeira, R., Mata, J., Tassinari, C., 2010. Petrology and geochemistry of lavas from Sal Island: implication for the variability of the Cape Verde magmatism. Comun. Geol. 97, 35–62.
Verhoef, J., Collette, B.J., Dañobeitia, J.J., Roeser, H.A., Roest, W.R., 1991. Magnetic anomalies off West-Africa (20–38°N). Mar. Geophys. Res. 13 (2), 81–103. https://doi.org/10.1007/BF00286283.

Vinnik, L., Silveira, G., Kiselev, S., Farra, V., Weber, M., Stutzmann, E., 2012. Cape Verde hotspot from the upper crust to the top of the lower mantle. Earth Planet. Sci. Lett. 319–320, 259–268. https://doi.org/10.1016/j.epsl.2011.12.017.

Voight, B., Widiwijayanti, C., Mattioli, G., Elsworth, D., Hidayat, D., Strutt, M., 2010. Magma-sponge hypothesis and stratovolcanoes: Case for a compressible reservoir and quasi-steady deep influx at Soufrière Hills Volcano, Montserrat. Geophys. Res. Lett. 37 https://doi.org/10.1029/2009GL041732.

Wallace, P.J., Plank, T., Bodnar, R.J., Gaetani, G.A., Shea, T., 2021. Olivine-hosted melt inclusions: a microscopic perspective on a complex magmatic world. Annu. Rev. Earth Planet. Sci. 49, 465–494. https://doi.org/10.1146/annurev-earth-082420-060506.

White, W.M., McBirney, A.R., Duncan, R.A., 1993. Petrology and geochemistry of the Galápagos Islands: portrait of a pathological mantle plume. J. Geophys. Res. 98 (B11), 19533–19563. https://doi.org/10.1029/93JB02018.

Wieser, P.E., Lamadrid, H., Maclennan, J., Edmonds, M., Matthews, S., Iacovino, K., et al., 2021. Reconstructing magma storage depths for the 2018 Kī̄lauean eruption from melt inclusion CO_2 contents: the importance of vapor bubbles. Geochem. Geophys. Geosyst. 22 https://doi.org/10.1029/2020GC009364.

Wilmart, E., Clocchiatti, R., Duchesne, J.-C., Touret, J.L.R., 1991. Fluid inclusions in charnockites from the Bjerkreim-Sokndal massif (Rogaland, southwestern Norway): fluid origin and in situ evolution. Contrib. Mineral. Petrol. 108, 453–462. https://doi.org/10.1007/BF00303449.

Wilson, D.J., Peirce, C., Watts, A.B., Grevemeyer, I., 2013. Uplift at lithospheric swells–II: is the Cape Verde mid-plate swell supported by a lithosphere of varying mechanical strength? Geophys. J. Int. 193, 798–819. https://doi.org/10.1093/gji/ggt034.

Zanon, V., 2015a. Conditions for mafic magma storage beneath fissure zones at oceanic islands. The case of São Miguel Island (Azores archipelago). In: Caricchi, L., Blundy, J.D. (Eds.), Chemical, Physical and Temporal Evolution of Magmatic Systems. The Geological Society of London, Special Publications, pp. 85–104, 422. https://doi.org/10.1144/SP422.4.

Zanon, V., 2015b. The magmatism of the Azores islands. Geol. Soc. Lond. Mem. 44 (1), 51–64. https://doi.org/10.1144/M44.5.

Zanon, V., Frezzotti, M.L., 2013. Magma storage and ascent conditions beneath Pico and Faial islands (Azores archipelago): a study on fluid inclusions. Geochem. Geophys. Geosyst. 14, 3494–3514. https://doi.org/10.1002/ggge.20221.

Zanon, V., Pimentel, A., Auxerre, M., Marchini, G., Stuart, F.M., 2020. Unravelling the magma feeding system of a young basaltic oceanic volcano. Lithos 352–353, 105325. https://doi.org/10.1016/j.lithos.2019.105325.

Web references

https://georoc.eu/georoc/new-start.asp.
https://sketchfab.com/WVUpetrology.